Density-functional analysis of spin exchange and ferroelectric polarization in $AgCrO_2$

E. J. Kan,[1] H. J. Xiang,[2] Y. Zhang,[1] C. Lee,[1] and M.-H. Whangbo[1]
[1]*Department of Chemistry, North Carolina State University, Raleigh, North Carolina 27695-8204, USA*
[2]*National Renewable Energy Laboratory, Golden, Colorado 80401, USA*
(Received 16 May 2009; revised manuscript received 11 August 2009; published 14 September 2009)

Density-functional calculations were carried out for $AgCrO_2$ to examine its spin exchange and ferroelectric polarization. In the multiferroic state of $AgCrO_2$ the triangular spin lattice of each CrO_2 layer forms parallel chains with helical-spin order. The spin exchange interactions of $AgCrO_2$ are strongly frustrated both within and between adjacent CuO_2 layers, which gives rise to the observed helical-spin order. The observed ferroelectric polarization of $AgCrO_2$ is not caused by individual helical-spin chains, but by the spiral-spin chain structures that propagate between the helical-spin chains.

DOI: 10.1103/PhysRevB.80.104417 PACS number(s): 75.80.+q, 71.20.−b, 77.80.−e

I. INTRODUCTION

In multiferroics driven by magnetic order, ferroelectric (FE) polarization appears in an ordered magnetic state with no inversion symmetry.[1–5] The magnetic-order-driven FE polarization in collinear-spin systems is discussed in terms of exchange striction,[6–8] and that in noncollinear-spin systems in terms of spin-orbit coupling (SOC).[9–11] Qualitatively, the FE polarization of a spiral-spin chain is described by the Katsura-Nagaosa-Balatsky (KNB) model,[12] according to which a chain with cycloid-spin order gives rise to FE polarization, but a chain with proper-screw or helical-spin order (hereafter, a helical-spin chain) [Fig. 1(a)] does not.

$AgCrO_2$ consists of CrO_2 triangular layers made up of edge-sharing CrO_6 octahedra with Cr^{3+} (d^3,S=3/2) ions [Fig. 1(b)]. Each CrO_2 layer has chains of edge-sharing CrO_6 octahedra running along the a, b, or (a+b) direction. Adjacent CrO_2 layers are stacked along the c direction with diamagnetic Ag^+ (d^{10}) ions intercalated between the CrO_2 layers to form linear O-Ag-O bridges such that there are three CrO_2 layers per unit cell [Fig. 1(c)]. $AgCrO_2$ exhibits FE polarization ($\sim$5 $\mu C/m^2$) in the magnetic ground state below $\sim$21 K, in which each triangular spin lattice (TSL) of Cr^{3+} ions separates into helical-spin chains of Cr^{3+} ions.[13,14] From the viewpoint of the KNB model, this finding is apparently puzzling. The FE polarization in $AgCrO_2$ and its isostructural analog $CuFeO_2$ (Refs. 15–17) has been explained by noting that a magnetic structure with C_2 rotation symmetry leads to FE polarization along the rotation axis.[18] Arima examined the possible directions of FE polarization in $CuFeO_2$ by analyzing the symmetry of the magnetic structure of an isolated FeO_2 layer composed of helical-spin chains,[17] to find that the direction of FE polarization depends on the orientation of the screw-rotation plane. Seki *et al.* presented a similar discussion for the FE polarization of $AgCrO_2$.[14]

An important question concerning $AgCrO_2$ is why its magnetic ground state has helical-spin chains. As depicted in Fig. 1(c), the spin exchange paths of $AgCrO_2$ include the intralayer exchange J_{NN}, J_{NNN}, and J_{ab} and the interlayer exchange J_c. In each CrO_2 layer, the nearest-neighbor (NN) helical-spin chains interact through J_{NN}, and the next-nearest-neighbor (NNN) chains through J_{NNN} and J_{ab} [Fig. 1(c)]. Between adjacent CrO_2 layers, the helical-spin chains interact through J_c [Fig. 1(c)]. In general, non-collinear-spin arrangements occur to reduce the extent of geometric spin frustration.[19] If the spin exchange other than J_{NN} is negligible [Fig. 1(c)], each CuO_2 layer should have the noncollinear 120° magnetic structure.[19] Given that the screw-rotation plane of each helical-spin chain is perpendicular to the plane of each CuO_2 layer, the spins are noncollinear along the interchain directions in each CrO_2 layer and along the interlayer directions. Thus, substantial geometric spin

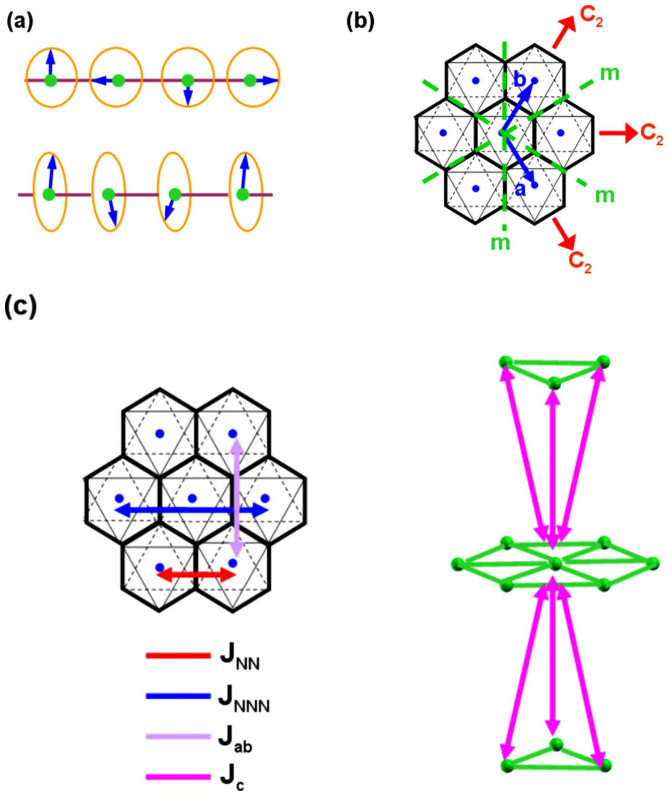

FIG. 1. (Color online) (a) Schematics of spiral-spin chains with cycloid-spin (top) and helical-spin (down) order. (b) A projection view of an isolated CrO_2 layer of $AgCrO_2$ showing the C_2 and S_2 symmetry axes. (c) A projection view of an isolated CrO_2 layer of $AgCrO_2$ showing the intralayer spin exchange paths J_{NN}, J_{NNN}, and J_{ab} (left), and a perspective view of three consecutive layers of Cr^{3+} ions showing the interlayer spin exchange J_c (right).

 ©2009 The American Physical Society

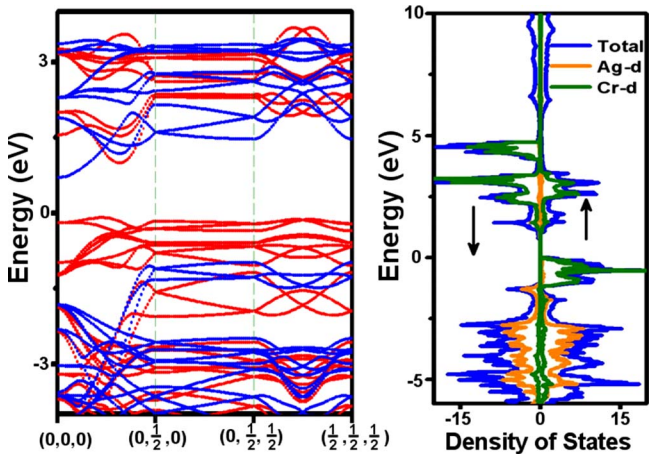

FIG. 2. (Color online). Electronic structure calculated for the FM state of $AgCrO_2$: (a) Dispersion relations of the up-spin and down-spin bands (red (light) and blue (dark) lines, respectively). (b) Total DOS plot and partial DOS plots for the Ag and Cr atoms.

frustration should exist within each CuO_2 layer and between adjacent CuO_2 layers. To verify this point, one needs to evaluate the values of J_{NN}, J_{NNN}, J_{ab}, and J_c by electronic structure calculations. Another important question about $AgCrO_2$ concerns the direction and magnitude of FE polarization expected for a TSL with helical-spin order. So far, the FE polarization predicted from the C_2-symmetry analysis[14,17] has not been confirmed by electronic structure calculations. Furthermore, it is important to see if the TSL has FE polarization along other symmetry-dictated directions. In the present work, we investigate these questions by performing density functional theory (DFT) calculations for $AgCrO_2$ with and without including spin-orbit coupling effects.

II. CALCULATIONS

Our spin-polarized DFT calculations employed the projector augmented wave method[20] encoded in the Vienna *ab initio* simulation package,[21] the local density approximation (LDA), and the plane wave cutoff energy of 400 eV. The LDA plus on-site repulsion U method (LDA+U) was employed to properly describe the electron correlation associated with the Cr 3*d* states.[22] The values of U=2.3 eV and J=0.96 eV on Cr reported in the literature[23] were adopted for our LDA+U calculations. The electronic structure of $AgCrO_2$ calculated for the ferromagnetic state is presented in Fig. 2, which shows that the ferromagnetic state is insulating with an indirect band gap. The band dispersion is strong in the *ab* plane but weak along the *c* direction [Fig. 2(a)], as expected for the layered structure of $AgCrO_2$. The plots of the density of states (DOS) reveal the presence of three electrons in the up-spin Cr 3*d* bands, which is consistent with the picture of high-spin Cr^{3+} (d^3) ions in $AgCrO_2$.

III. SPIN EXCHANGE INTERACTIONS

The four spin exchange parameters, J_{NN}, J_{NNN}, J_{ab} and J_c can be evaluated by examining the five ordered spin states of $AgCrO_2$ (i.e., the FM, AF1, AF2, AF3, and AF4 states)

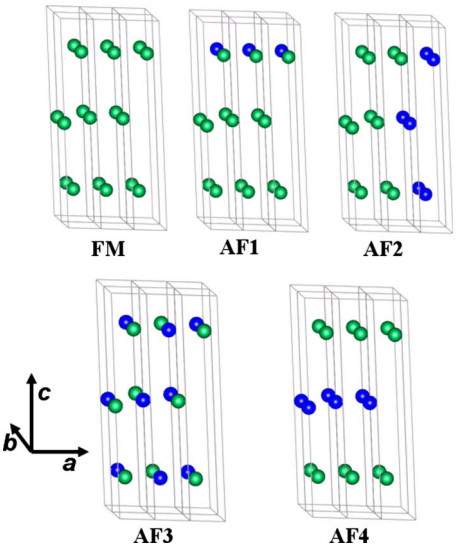

FIG. 3. (Color online). Five ordered spin states of $AgCrO_2$ employed to extract the four spin exchange parameters J_{NN}, J_{NNN}, J_{ab} and J_c. For simplicity, only the Cr^{3+} ions are shown. The spin-up and spin-down Cr^{3+} ion sites are represented by green (light) and blue (dark) spheres, respectively.

defined in Fig. 3 in terms of a $3\times2\times1$ supercell. Table I summarizes the relative energies of these states per $3\times2\times1$ supercell, i.e., per 18 f.u., determined from our LDA+U calculations. To extract the values of the spin exchange parameters J_{NN}, J_{NNN}, J_{ab} and J_c, we express the total spin exchange interaction energies of the five ordered spin states in terms of the spin Hamiltonian,

$$\hat{H} = \sum_{i<j} J_{ij} \hat{S}_i \cdot \hat{S}_j, \tag{1}$$

where J_{ij} (=J_{NN},J_{NNN},J_{ab},J_c,) is the spin exchange parameter for the spin exchange interaction between the spin sites i and j, while $\hat{S}_i$ and $\hat{S}_j$ are the spin angular momentum operators at the spin sites i and j, respectively. Then, by applying the energy expressions obtained for spin dimers with N unpaired spins per spin site (in the present case, N=3),[24] the total spin exchange energies (per 18 f.u.) of the five ordered spin states are expressed as

$$E(\mathrm{FM}) = -(N^2/4)(-54J_{NN} - 54J_{NNN} - 54J_{ab} - 54J_c),$$

$$E(\mathrm{AF1}) = -(N^2/4)(-30J_{NN} - 54J_{NNN} - 30J_{ab} - 18J_c),$$

$$E(\mathrm{AF2}) = -(N^2/4)(-6J_{NN} - 6J_{NNN} + 18J_{ab} - 22J_c),$$

TABLE I. Relative energies in meV of the five ordered spin states of $AgCrO_2$ determined from LDA+U calculations.

FM	0
AF1	178
AF2	342
AF3	489
AF4	309

TABLE II. Values of the spin exchange parameters in meV extracted from the LDA+U calculations.

J_{NN}	1.10
J_{NNN}	0.85
J_{ab}	−0.50
J_c	1.80

$$E(\mathrm{AF3}) = -(N^2/4)(+18J_{NN} - 6J_{NNN} - 6J_{ab} - 6J_c),$$

$$E(\mathrm{AF4}) = -(N^2/4)(-54J_{NN} - 54J_{NNN} - 54J_{ab} + 18J_c). \quad (2)$$

When the relative energies of the five ordered magnetic states determined from the LDA+U calculations are mapped onto the corresponding energies determined from the spin Hamiltonian, we obtain the values of J_{NN}, J_{NNN}, J_{ab} and J_c summarized in Table II.

It is noted from Table I that the intralayer spin exchanges J_{NN} and J_{NNN} are substantially antiferromagnetic so that, within each CuO_2 layer, spin frustration occurs in every triangle of J_{NN}, in every triangle of J_{NNN}, and along every edge-sharing chain due to J_{NN} and J_{NNN}. Furthermore, the interlayer spin exchange J_c is strongly antiferromagnetic so that, between adjacent CuO_2 layers, spin frustration occurs in every isosceles triangle made up of J_{NN} and J_c. This confirms our suggestion that the helical-spin chains of $AgCrO_2$ arise from strong inter- and intralayer geometric spin frustration.

IV. FERROELECTRIC POLARIZATION

A. Dependence on the arrangement of helical-spin chains

The propagation vector of the helical-spin chains in $AgCrO_2$ was found to be $(q, q, 0)$ with $q=1/3$,[13,14] namely, the chains run along the $(a+b)$ direction with screw-rotation angle of 120°. Given the trigonal symmetry of $AgCrO_2$, the $(a+b)$ direction is equivalent to the a or b direction [Fig. 1(b)]. Without loss of generality, therefore, the helical-spin chains can be assumed to run along the a direction with the screw-rotation angle 120° and the clockwise rotation of the spins along the a direction.

TABLE III. Ferroelectric polarizations (in units of $\mu C/m^2$) determined for the helical-spin states Q_a, Q_{a+b}, and Q_{-a+b} of $AgCrO_2$ from LDA+U+SOC calculations.

	Q_a	Q_{a+b}	Q_{-a+b}
(001)	$P_{\perp(a+b)}=-75.5$	$P_{\parallel a}=140.6$	$P_{\perp b}=75.5$
(001)	$P_{\parallel(a+b)}=0.0$	$P_{\perp a}=0.0$	$P_{\parallel b}=0.0$
[001]	$P_{\parallel c}=32.3$	$P_{\parallel c}=0.0$	$P_{\parallel c}=32.3$

For each CrO_2 layer we consider three different ordered magnetic structures, which are described by the propagation vectors $Q_a=(1/3,0,0)$, $Q_{a+b}=(1/3,1/3,0)$ and $Q_{-a+b}=(-1/3,1/3,0)$ (Fig. 4). Here the repeat patterns are generated by using the direct vectors a, b, and c. In the Q_a state, the helical-spin chains repeat along the b direction without changing the screw-rotation angle [Fig. 4(a)]. In the Q_{a+b} state, the helical-spin chains repeat along the b direction while advancing the screw-rotation clockwise by 120° [Fig. 4(b)]. In the Q_{-a+b} state, the screw-spin chains repeat along the b direction while advancing the screw-rotation anticlockwise by 120° [Fig. 4(c)].

On the basis of LDA+U calculations, we evaluate the FE polarizations for the Q_a, Q_{a+b}, and Q_{-a+b} states by using the Berry phase method[25] and the (3a, 3b, c) supercell and also by fully relaxing the atom positions. These calculations do not lead to any FE polarization, so the FE polarizations of $AgCrO_2$ is not explained by the exchange striction mechanism. We then evaluate the FE polarizations of the three states by performing LDA+U+SOC calculations for the structures optimized from the LDA+U calculations. These calculations show substantial FE polarization for the Q_a, Q_{a+b}, and Q_{-a+b} states (Table III) so that, as found for spiral-spin chain systems,[9–11] SOC is essential for the FE polarization of $AgCrO_2$. This is so because SOC allows the ordered magnetic state with no inversion symmetry to adopt its optimal electron density distribution.

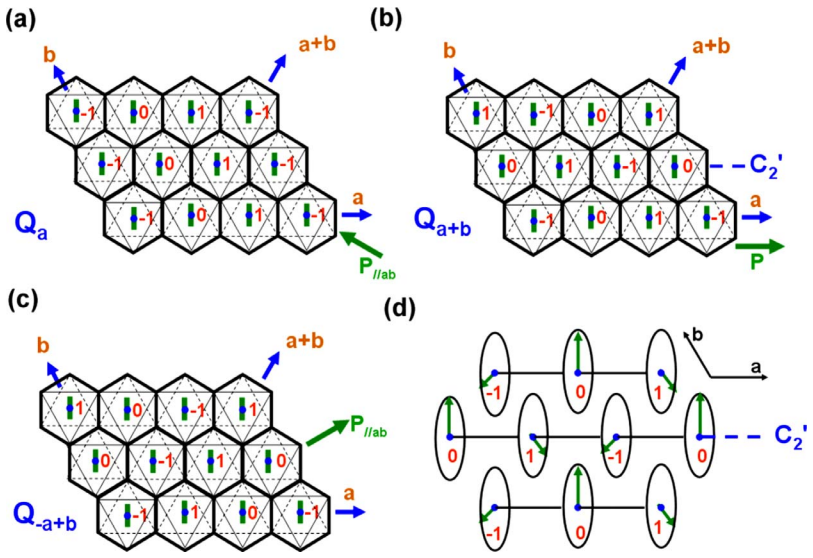

FIG. 4. (Color online). Schematic representations of the three magnetic states generated by repeating the screw-spin chains running along the a direction: (a) Q_a, (b) Q_{a+b} and (c) Q_{-a+b}. The number 0, 1 and −1 in the CrO_6 octahedra show that the screw-rotation angle in their screw-rotation planes are 0°, 120° and −120°, respectively. (d) Perspective view of the screw-spin chains in the Q_{a+b} state emphasizing the presence of C_2 symmetry.

It should be emphasized that the nonzero FE polarization calculated for the Q_a, Q_{a+b}, and Q_{-a+b} states does not arise from individual helical-spin chains. To simulate an isolated helical-spin chain, we constructed a hypothetical system in which there is only one helical-spin chain in the (3a, 3b, c) supercell by replacing all Cr^{3+} ions with Al^{3+} ions except for one helical-spin chain. Our LAD+U+SOC calculations for this system show that the FE polarization is practically zero as expected from the KNB model. Therefore, the nonzero FE polarization calculated for the Q_a, Q_{a+b} and Q_{-a+b} states does not arise from the individual helical-spin chains, but from the spin arrangements between these chains.

B. Dependence on the symmetry of magnetic structure

It is of interest to examine how the direction of the calculated FE polarization in the Q_a, Q_{-a+b} and Q_{a+b} states is related to the symmetry of their spin arrangements. In the Q_{a+b} state, the FE polarization occurs only along the a direction (i.e., $P_{\|a}=140.6\ \mu C/m^2$). Given the equivalence of the $(a+b)$ and a directions of the TSL [Fig. 1(b)], this result confirms Arima's analysis for the case of the $(q, q, 0)$ propagation of the screw-spin chain,[17] for which the screw-spin chains are along the $(a+b)$ direction and the magnetic structure of the TSL has C_2 symmetry (i.e., C_2 rotation followed by time reversal) along the chain direction [Figs. 4(b) and 4(d)]. The calculated value of $P_{\|a}=140.6\ \mu C/m^2$ is greater than the experimental value ($\sim 5\ \mu C/m^2$) (Refs. 14) by a factor of ~ 30.

In the Q_a state, the electric polarization is nonzero along the $\perp(a+b)$ direction in the ab plane (i.e., $P_{\perp}(a+b)=75.5\ \mu C/m^2$) [Fig. 4(a)] and also along the c direction (i.e., $P_{\|c}=32.3\ \mu C/m^2$). Note that the $\perp(a+b)$ direction is parallel to a mirror plane [Fig. 1(b)]. The FE polarization of the Q_{-a+b} state is similar to that of the Q_a state, except that its ab-plane component of the FE polarization is perpendicular to the b direction [Fig. 4(c)]. The $\perp b$ direction in the ab-plane is also parallel to a mirror plane of the TSL [Fig. 1(b)]. The magnetic structure of the TSL has C_2 symmetry in the Q_{a+b} state [Figs. 4(b) and 4(d)], as found by Arima.[17] However, magnetic structures of the Q_a and Q_{-a+b} states have no global symmetry, but give rise to a nonzero FE polarization as described above. The origin of this puzzling observation is analyzed in the next section.

C. Hidden symmetry and ferroelectric polarization

In the Q_{a+b} state, the interchain spiral-spin propagates along the b and the $(a+b)$ directions with opposite senses of rotation [Fig. 4(b)]. In the Q_a and Q_{-a+b} states, the interchain spiral-spin propagates only in one direction, i.e., the $(a+b)$ direction in the Q_a state [Fig. 4(a)], and the b direction in the Q_{-a+b} state [Fig. 4(c)]. To discuss the FE polarization in the Q_a state, we present in Fig. 5(a) two "ribbons" of edge-sharing CrO_6 octahedra running along the interchain spiral-spin direction [i.e., the $\|(a+b)$ direction]. They were taken from the magnetic structure of the TSL in the Q_a state [Fig. 4(a)]. For simplicity, such ribbons will be referred to as the $\|(a+b)$-ribbons.

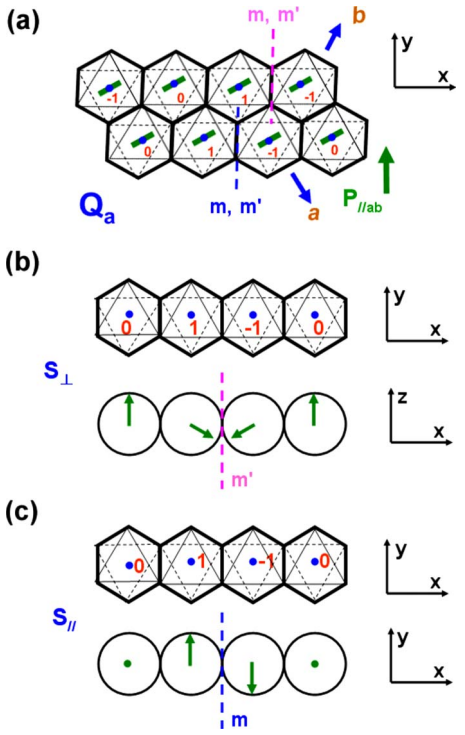

FIG. 5. (Color online). (a) Two ribbon chains of edge-sharing CrO_6 octahedra along the $\|(a+b)$ direction that contain the interchain spiral-spin structure, which were taken from the magnetic structure of the Q_a state presented in Fig. 4(a). (b) The perpendicular spin component, $\mathbf{S}_{\perp}$, at each spin site of an isolated $\|(a+b)$ ribbon in the state Q_a. (c) The parallel spin component, $\mathbf{S}_{\|}$, at each spin site of the $\|(a+b)$ ribbon in the state Q_a.

The NN interactions between the upper and lower $\|(a+b)$-ribbons of Fig. 5(a) occur along the a and b directions. These interribbon interactions involve the helical spins along the a direction, and the collinear spins along the b direction. Therefore, these interribbon interactions do not give rise to FE polarization. Consequently, every $\|(a+b)$-ribbon, which is perpendicular to the mirror plane, contributes independently to the FE polarization of the TSL, and all the $\|(a+b)$-ribbons are identical in nature. Nevertheless, the spiral-spin pattern in each $\|(a+b)$-ribbon presents no apparent symmetry that can be used to predict the direction of FE polarization.

Thus, as presented in Figs. 5(b) and 5(c), we decompose the spin vectors $\mathbf{S}$ at the spin sites of the $\|(a+b)$-ribbon into two parts, i.e., the perpendicular component $\mathbf{S}_{\perp}=\mathbf{S}_x+\mathbf{S}_z$ and the parallel component $\mathbf{S}_{\|}=\mathbf{S}_y$, with respect to the mirror plane. Here the coordinate axes are chosen such that the xz-plane contains the $\|(a+b)$-ribbon plane with the z axis perpendicular to the ribbon. Then, the $\mathbf{S}_{\perp}$ components of the spin sites form a cycloidlike spiral-spin chain along the $(a+b)$ direction [Fig. 5(b)], which has the m' symmetry (i.e., mirror-reflection followed by time reversal). The cycloidlike spin chain gives rise to FE polarization along the c direction ($P_{\|c}\neq 0$) according to the KNB rule. The $\mathbf{S}_{\|}$ components of the spin sites form a collinear-spin pattern as depicted in Fig. 5(c), which has the mirror-plane symmetry m. The latter requires that the associated FE polarization lie in the mirror

plane. This accounts for why the FE polarization of the Q_a state is along the $\perp(a+b)$ direction in the ab-plane ($P_{\perp(a+b)} \neq 0$). Note that the mirror plane of the $\|(a+b)$-ribbon chain, providing the m' and m symmetry for the $\mathbf{S}_\perp$ and $\mathbf{S}_\|$ spin components, shifts its position along the $(a+b)$ direction [Fig. 5(a)] on going from one ribbon chain to its adjacent chain. As a result, there is no global symmetry in the magnetic structure of the TSL. The FE polarization of the Q_{-a+b} state is similarly explained.

V. CONCLUDING REMARKS

$AgCrO_2$ possesses strong intra- and inter-layer geometric spin frustration, which leads to the observed helical-spin chain order. The FE polarization of $AgCrO_2$ with helical-spin chain order originates from the spiral-spin structures that propagate between the helical-spin chains. $AgCrO_2$ can have FE polarization not only along its C_2 rotational axis but also in its mirror plane.

ACKNOWLEDGMENTS

The research was supported by the Office of Basic Energy Sciences, Division of Materials Sciences, U.S. Department of Energy, under Grant No. DE-FG02-86ER45259 and also by computing resources at the NERSC and the HPC Centers.

[1] M. Fiebig, J. Phys. D **38**, R123 (2005).
[2] S.-W. Cheong and M. Mostvoy, Nature Mater. **6**, 13 (2007).
[3] T. Kimura, T. Goto, H. Shintani, K. Ishizaka, T. Arima, and Y. Tokura, Nature (London) **426**, 55 (2003).
[4] N. Hur, S. Park, P. A. Sharma, J. S. Ahn, S. Guha, and S.-W. Cheong, Nature (London) **429**, 392 (2004).
[5] Y. Tokura, Science **312**, 1481 (2006).
[6] L. C. Chapon, P. G. Radaelli, G. R. Blake, S. Park, and S.-W. Cheong, Phys. Rev. Lett. **96**, 097601 (2006).
[7] Y. J. Choi, H. T. Yi, S. Lee, Q. Huang, V. Kiryukhin, and S.-W. Cheong, Phys. Rev. Lett. **100**, 047601 (2008).
[8] Y. Zhang, H. J. Xiang, and M.-H. Whangbo, Phys. Rev. B **79**, 054432 (2009).
[9] H. J. Xiang, S. H. Wei, M.-H. Whangbo, and J. L. F. Da Silva, Phys. Rev. Lett. **101**, 037209 (2008).
[10] H. J. Xiang and M.-H. Whangbo, Phys. Rev. Lett. **99**, 257203 (2007).
[11] A. Malashevich and D. Vanderbilt, Phys. Rev. Lett. **101**, 037210 (2008).
[12] H. Katsura, N. Nagaosa, and A. V. Balatsky, Phys. Rev. Lett. **95**, 057205 (2005).
[13] Y. Oohara, S. Mitsuda, H. Yoshizawa, N. Yaguchi, H. Kuriyama, T. Asana, and M. Mekata, J. Phys. Soc. Jpn. **63**, 847 (1994).
[14] S. Seki, Y. Onose, and Y. Tokura, Phys. Rev. Lett. **101**, 067204 (2008).
[15] T. Kimura, J. C. Lashley, and A. P. Ramirez, Phys. Rev. B **73**, 220401(R) (2006).
[16] T. Nakajima, S. Mitsuda, S. Kanetsuki, K. Prokes, A. Podlesnyak, H. Kimura, and Y. Noda, J. Phys. Soc. Jpn. **76**, 043709 (2007).
[17] T. Arima, J. Phys. Soc. Jpn. **76**, 073702 (2007).
[18] M. Mostovoy, Phys. Rev. Lett. **96**, 067601 (2006).
[19] J. E. Greedan, J. Mater. Chem. **11**, 37 (2001); D. Dai and M.-H. Whangbo, J. Chem. Phys. **121**, 672 (2004).
[20] P. E. Blöchl, Phys. Rev. B **50**, 17953 (1994); G. Kresse and D. Joubert, *ibid.* **59**, 1758 (1999).
[21] G. Kresse and J. Furthmüller, Comput. Mater. Sci. **6**, 15 (1996); Phys. Rev. B **54**, 11169 (1996).
[22] A. I. Liechtenstein, V. I. Anisimov, and J. Zaanen, Phys. Rev. B **52**, R5467 (1995).
[23] I. I. Mazin, Phys. Rev. B **75**, 094407 (2007).
[24] D. Dai and M.-H. Whangbo, J. Chem. Phys. **114**, 2887 (2001); **118**, 29 (2003).
[25] R. D. King-Smith and D. Vanderbilt, Phys. Rev. B **47**, 1651 (1993); R. Resta, Rev. Mod. Phys. **66**, 899 (1994).